Journal of Power Sources 196 (2011) 5922–5927

Contents lists available at ScienceDirect

Journal of Power Sources

journal homepage: www.elsevier.com/locate/jpowsour

Short communication

Characterization and performance of UNS S63019 (21-4N) as bipolar plate material in a simulated polymer electrolyte membrane fuel cell environment

Andrew G. Howell[a,*], Heli Wang[b], Scott W. Cowley[a], John A. Turner[b]

[a] Colorado School of Mines, Department of Chemistry and Geochemistry, 1600 Maple Street, Golden, CO 80401, USA
[b] National Renewable Energy Laboratory, Hydrogen Technologies and Systems Center, 1617 Cole Boulevard, Golden, CO 80401, USA

ARTICLE INFO

Article history:
Received 7 January 2011
Received in revised form 11 February 2011
Accepted 17 February 2011
Available online 5 March 2011

Keywords:
Bipolar plate
UNS S63019
PEMFC
ICR
Corrosion
Stainless steel

ABSTRACT

The austenitic stainless steel UNS S63019 was evaluated regarding its potential as bipolar plate material in a polymer electrolyte membrane fuel cell (PEMFC) environment. Segregated grains of niobium carbide (NbC_x) were identified in polished cross-sections of the alloy, offering a possible pathway for enhanced electrical conductivity through the passive surface oxide. Additionally, the alloy was tested for corrosion resistance in a simulated PEMFC environment. It was considered that perhaps the elevated nitrogen concentration in the alloy would provide some benefit for corrosion resistance.

Results for interfacial contact resistance (ICR) testing of the air-formed surface film on UNS S63019 showed decreased electrical conductivity as compared to UNS S30400. Niobium carbide particles did not improve film conductivity due to a non-conductive niobium oxide layer that formed on the surface. Corrosion resistance of the alloy was also poor as compared with UNS S30400, demonstrating that elevated nitrogen concentration in the alloy was not adequate in itself to enhance corrosion resistance. Poor corrosion resistance was attributed primarily to high carbon content in the alloy which combined with a significant amount of chromium to form carbides.

1. Introduction

In recent years, many materials have been evaluated for use as bipolar plates in polymer electrolyte membrane fuel cells (PEMFC), including stainless steels [1,2]. One of the more problematic issues is poor corrosion resistance in the fuel cell environment, which prevents stable, long-term fuel cell operation. A second problem is that sufficient electrical conductivity at the bipolar plate interface is necessary to reduce resistive losses during operation. Stainless steels have promising characteristics due to good corrosion resistance in many aqueous environments; however, this is accomplished via formation of a thin film of chromium oxide that is not electrically conductive. The passive film that forms on stainless steels is thin, typically less than 5 nm, and primarily composed of chromium oxide [3]. Transport of electrons across this electrically resistive oxide is slow, leading to efficiency losses in the cell. Stainless steels alloyed with greater concentrations of chromium, nickel and molybdenum can provide improved corrosion resistance by forming a thicker or more comprehensive oxide film, but this limits electron transport even further. Efforts have been made to address these opposing features by employing surface treatments that provide conductive pathways through the non-conductive oxide film, and by incorporating constituents into the bulk alloy that may also serve this purpose [4–7]. Incorporation of electrically conductive particles within the passive chromium oxide film may provide pathways for electron transport while maintaining excellent corrosion resistance [4,8,9].

Bipolar plate materials for accelerated PEMFC testing are commonly exposed to a dilute sulfuric acid aqueous environment with a small amount of fluoride ion. This solution simulates the environment found in a PEMFC; sulfate and fluoride can leach from the polymer electrolyte membrane, and oxidation of hydrogen gas during operation routinely generates an acidic environment. Specific experimental environments that have been used for testing stainless steels include 0.1 M H_2SO_4 + 2 mg L^{-1} F^- at 80 °C, 1 M H_2SO_4 + 2 mg L^{-1} F^- at 70 °C, and pH 2.3 and 4.3 solutions of sulfuric acid with 2 mg L^{-1} F^- at 80 °C [10–12]. The more concentrated acid solutions are used to represent aggressive PEMFC environments for accelerated testing purposes, and the corrosion resistance of lower-alloyed stainless steels in these environments has been relatively poor. Surface treatments to enhance corrosion resistance of these alloys by providing higher Cr, Ni, Mo, and/or N may be required.

An austenitic stainless steel alloy, UNS S63019 (also referred to as 21-4N), was tested for suitability as a bipolar plate material in PEMFC application. S63019 stainless steel is commonly used where hot strength, corrosion resistance, and structural stability at high temperatures are required; a common application is the inlet and exhaust valves of heavy duty diesel engines in trucks. The com-

* Corresponding author. Tel.: +1 303 275 4697; fax: +1 303 275 2905.
E-mail address: andrew.howell@nrel.gov (A.G. Howell).

0378-7753/$ – see front matter © 2011 Elsevier B.V. All rights reserved.
doi:10.1016/j.jpowsour.2011.02.055

Table 1
Chemical composition of UNS S63019 and 30,400.

	Fe	Cr	Mn	Ni	Nb	W	C	N	Mo	Si	Cu	V
S63019												
Weight%	61.66	20.60	9.70	3.63	1.83	0.87	0.541	0.46	0.26	0.21	0.14	0.053
Atom%	59.48	21.34	9.54	3.33	1.06	0.25	2.42	1.77	0.15	0.40	0.12	0.05
S30400												
Weight%	71.47	18.3	1.3	8.1	–	–	0.05	0.031	0.36	0.36	–	–

mon stainless steel UNS S30400 was also tested for comparison purposes. The compositions of the materials tested are listed in Table 1.

The influence of high nitrogen concentration (0.46 weight%) and the presence of niobium (1.83 weight%) were of particular interest regarding corrosion resistance and their influence on electrical conductivity of the passive surface film. Nitrogen has been found to reduce susceptibility to corrosion in many aqueous environments [13]. The presence of isolated grains of niobium carbide in the alloy matrix provided an opportunity to evaluate whether improved electrical conductivity might be achieved in the passive film due to these grains. Niobium carbide has been reported to have good conductivity, although a numerical value for its conductivity was not reported [4].

2. Experimental

2.1. Materials and preparation

The S63019 alloy material and melt chemistry were supplied by BGH Edelstahl Freital GmbH of Dresden, Germany. The S30400 alloy was purchased from Metal Samples of Munford, Alabama, USA. The S63019 coupons were prepared from bar stock with 2.11 cm^2 surface area on each side, ~0.2 cm thickness. The S30400 coupons were prepared with 2.37 cm^2 surface area on each side, ~0.2 cm thickness. Prior to interfacial conductivity resistance (ICR) measurements, the coupons were ground to 600-grit finish with SiC abrasive paper, rinsed with acetone and dried with nitrogen gas. After ICR measurements, the coupons were fabricated into working electrodes for polarization testing according to the procedure of Wang et al. [14].

Samples analyzed by scanning electron microscopy, after electrochemical testing, were removed from the fabricated electrode and examined directly. Additional metallurgical imaging and analysis of the S63019 surface required polishing the coupons to 0.05-μm finish with alumina.

2.2. Characterizations

A Hitachi model 3000N scanning electron microscope (SEM) with a tungsten filament (operated at 5 to 20 kV), and equipped with secondary and backscattered electron detectors, was used to image specimens at magnification. Energy-dispersive X-ray analyses (EDX) were performed with an accessory Oxford Instruments INCA 250 spectrometer. X-ray diffraction (XRD) measurements were accomplished with a Philips X-ray Diffractometer using Cu K-alpha radiation (1.540562 Å) in symmetric 2-theta mode. A Kratos X-ray Photoelectron Spectroscopy (XPS) system with hemispherical analyzer and Al K-alpha source radiation at 1486.6 eV was used for surface analysis; surface layers were removed by sputtering with an argon ion beam at 45° incidence to the sample.

2.3. Electrochemistry

Electrochemical tests were carried out in a simulated fuel cell environment containing sulfuric acid with 2 ppm F^- at 70 °C. Testing was done at both 1 M and 0.1 M H_2SO_4 for S63019, to evaluate the impact of acid concentration on the performance, but only in 1 M H_2SO_4 for S30400. A controlled temperature bath was used to maintain the solution to within ±1 °C. Air was bubbled into the solution to simulate the PEMFC cathode environment, and hydrogen was used to simulate the anode environment.

For electrochemical testing, a three-electrode cell was used with a saturated calomel electrode (SCE) as reference and platinum sheet as counter electrode. A computer-controlled Solartron 1287 was employed for the measurements. For both the potentiodynamic and the potentiostatic polarization tests, the electrode was stabilized at open circuit potential (OCP) for at least 5 min before proceeding. Potentiodynamic tests were accomplished by scanning from OCP in the anodic direction at a rate of 1 mV s^{-1}. Potentiostatic tests were performed conventionally by applying a specific potential, −0.1 V vs. SCE, to represent the PEMFC anodic environment (with hydrogen sparging), and +0.6 V vs. SCE was used to represent the cathodic environment (with air sparging), and recording the current response.

2.4. Interfacial contact resistance (ICR)

ICR measurements were carried out according to the method of Wang et al. [14]. To summarize, a test sample was placed between two pieces of carbon paper, which was between two gold-coated copper plates. A current between the plates was established at 1.000 A, and voltage change with respect to a change in the compaction force was measured. Measurements were taken starting with maximum applied pressure and reducing the pressure in defined increments. The ICR of the carbon paper/gold surface was measured to provide blank correction for calculations of the carbon paper/sample interface ICR. The dependence of ICR on pressure was plotted.

3. Results and discussion

3.1. Microstructure of S63019

Islands of niobium carbide (NbC_x) were present in the S63019 alloy matrix (Fig. 1). Note that the NbC_x grains are in the 2–10 μm size range, and therefore are much thicker than the 2–4 nm oxide film typically present on stainless steels. These particles were analyzed by EDX and confirmed that Nb and C were the primary elements present, but as EDX analysis is semiquantitative, an Nb:C ratio could not be accurately determined (Fig. 2). Chromium carbides (Cr_xC_y), also identified by EDX, were present as small particles in the etched surface; $Cr_{23}C_6$ is a typical composition (Figs. 3 and 4). Note the presence of an abundance of small pits in the polished-and-etched surface of Fig. 4, indicating the limited corrosion resistance of S63019.

3.2. XRD

XRD results for S63019 are shown in Fig. 5. The presence of niobium carbide (NbC) and austenite (face-centered cubic crystal structure) were confirmed. There was no evidence of nitrogen incorporated into the FCC structure to form expanded austenite.

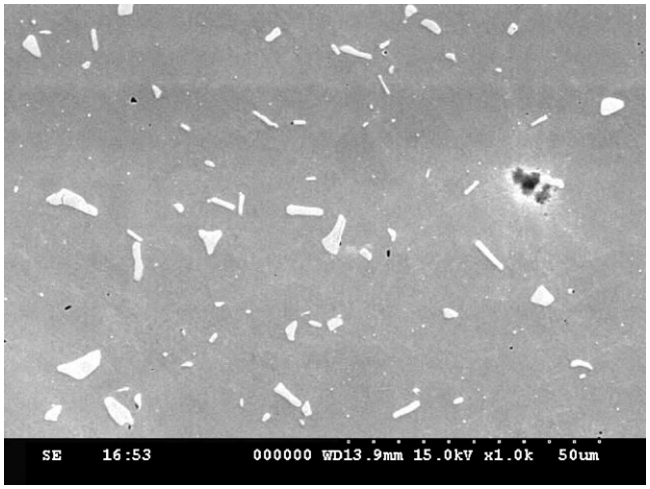

Fig. 1. Secondary electron SEM image of S63019 polished to 0.5-μm finish. The bright particles embedded in the matrix are primarily NbC_x.

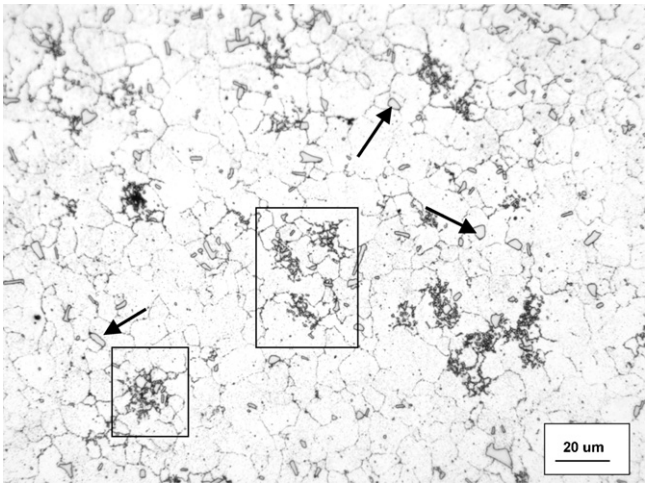

Fig. 3. Etched microstructure, S63019, reflected light, 400× magnification. NbC_x (arrows) and chromium carbides (clusters in boxes) are present. Etchant: equal concentrations of HCl, HNO_3, and H_2O.

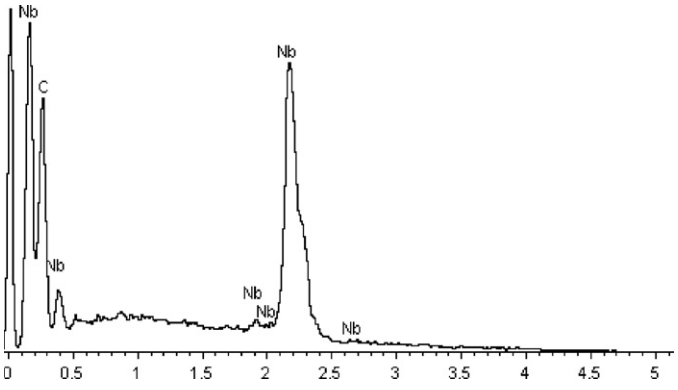

Fig. 2. Energy-dispersive X-ray analysis (microbeam) of NbC_x particle in Fig. 1, confirming the presence of Nb and C.

Fig. 4. Etched microstructure, S63019, SEM backscattered electron image. The larger light particles are NbC_x (arrows), the smaller light particles are chromium carbides (box).

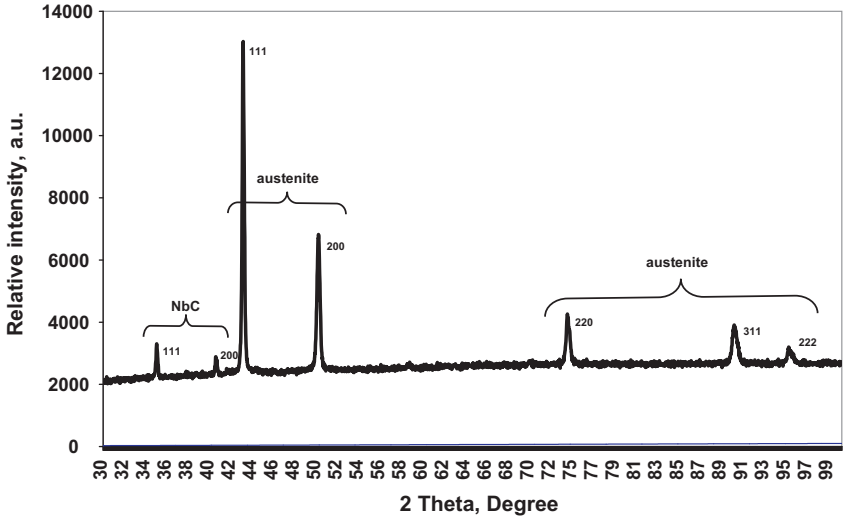

Fig. 5. X-ray diffraction data for S63019 demonstrating the presence of NbC and an austenitic (FCC) crystal structure for the alloy (600-grit grinding).

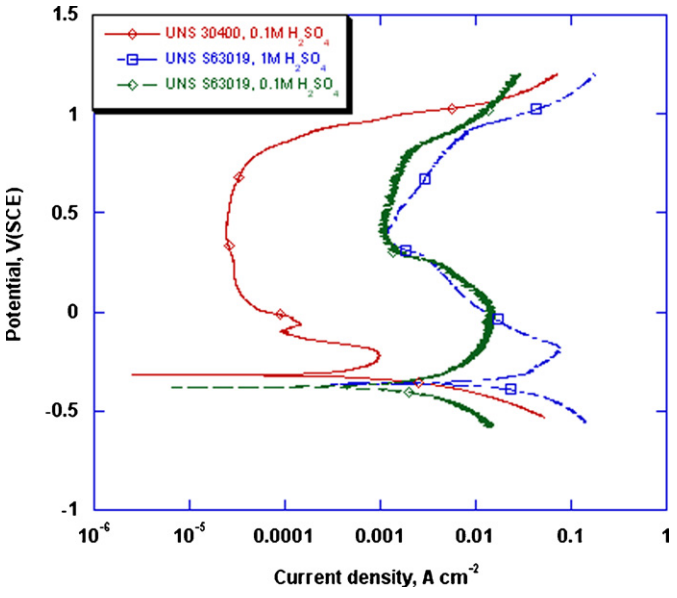

Fig. 6. Potentiodynamic polarization of S30400 and S63019 in 1M H2SO4 and S63019 in 0.1 M H_2SO_4 in a hydrogen-saturated solution. The current density for S30400 is much lower than S63019.

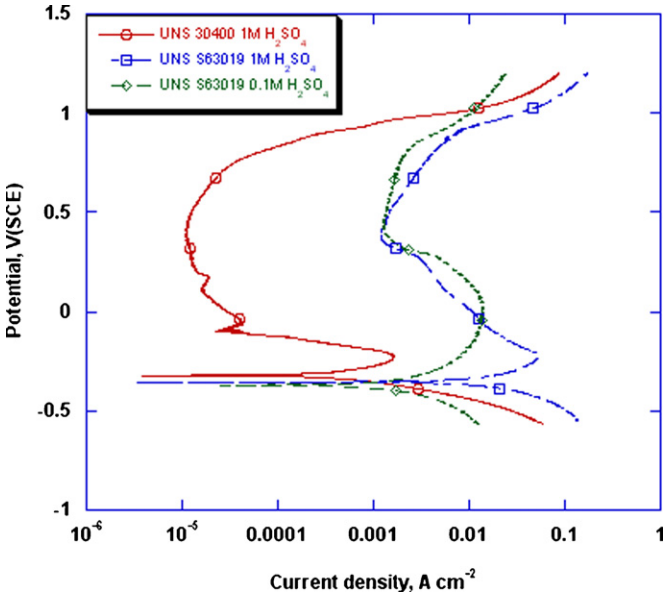

Fig. 7. Potentiodynamic polarization of 30400 and S63019 in 1M H2SO4 and S63019 in 0.1 M H_2SO_4 in an oxygen-saturated solution. The current density for S30400 is much lower than S63019.

3.3. XPS

XPS results for the surface and base metal after etching are shown in Table 2.

Niobium oxide(s) and niobium carbide(s) were identified by XPS, with increased concentration of oxygen prior to removal of surface layers by sputtering, and increased carbide concentration after surface layers were removed. Nitrogen was identified at trace concentrations in nitride form. Chromium analyses confirmed the presence of the typical passive chromium oxide layer on the original surface, with most of the oxide removed after sputtering.

3.4. Polarization behavior

Potentiodynamic polarization results are shown in Figs. 6 and 7. With H_2 sparging, alloy S30400 showed stability at a current density of about 2×10^{-4} A cm^{-2}, whereas S63019 did not show stability and had a minimum current density of about 9×10^{-3} A cm^{-2} in both 1 M and 0.1 M H_2SO_4. Results with air sparging were similar.

Potentiostatic polarization results are shown in Figs. 8 and 9. In an H_2 environment at −0.1V, 30400 reached a minimum passivation at a current density of 1.25×10^{-5} A cm^{-2}, whereas for S63019 in both 1 M and 0.1 M H_2SO_4, a much greater minimum current density, in the range of 1×10^{-2} A cm^{-2}, was measured. In the air environment, S30400 passivated at 1×10^{-5} A cm^{-2} and S63019 had minimum current densities of 7.5×10^{-4} and 2.5×10^{-4} A cm^{-2} in 0.1 M and 1 M H_2SO_4, respectively.

In all cases, electrochemical testing results in the aggressive test solutions for both S30400 and S63019 were unsatisfactory in terms of minimum current density and for stability requirements for PEMFC use, with passive film breakdown in a relatively short time (<7 hours). However, 30400 performed considerably better than S63019 overall, and its performance in an actual PEMFC could not be ruled inadequate based solely on testing in aggressive solutions.

SEM observation of the cathodic potentiostatic polarization test of S63019 in 0.1 M H_2SO_4 demonstrated significant intergranular corrosion, as well as accelerated metal loss near clusters of chromium carbides (Fig. 10).

3.5. ICR

ICR was measured on the air-formed oxide for both alloys. As shown in Fig. 11, the oxide film on S63019 was less electrically conductive than that on S30400.

3.6. Discussion

It was anticipated that the presence of elevated nitrogen concentration might contribute to enhance corrosion resistance of S63019. However, the corrosion resistance of S63019 was poor compared with S30400. This poor corrosion resistance of S63019 is attributed primarily to the high carbon concentration in the alloy, such that a significant amount of chromium reacted with carbon to form chromium carbides (Figs. 3 and 4). As a result, inadequate chromium concentration was present to form and maintain

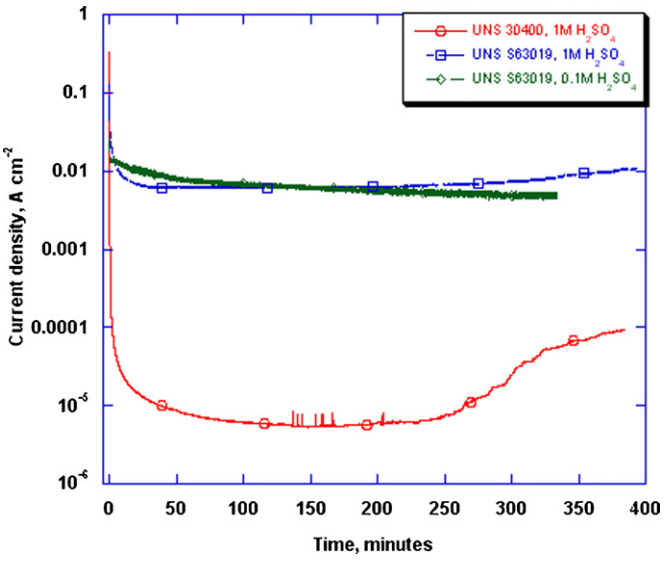

Fig. 8. Potentiostatic polarization of S30400 and S63019 in 1 M H_2SO_4 and S63019 in 0.1 M H_2SO_4 in a hydrogen-saturated solution. The current density for S30400 is much lower than for S63019.

Table 2
XPS data for as-polished and etched surfaces (the element whose binding energy was measured is in bold).

Surface peaks			Peaks after 180-s sputtering		
Binding energy (eV)	Signal strength	Primary/probable compound(s)	Binding energy (eV)	Signal strength	Primary/probable compound(s)
204.2	Small	NbO	203.8	Small	NbO
206.9	Small	Nb_2O_5	206.6	Small	NbC
283.3	Small	NbC or CrC_x	283.0	Small	NbC or CrC_x
285.4	Large	Adventitious C	284.9	Small	NbC
396.6	Trace	N (nitrides) of Nb, Cr, Ti, W or Si	397.5	Trace	N (nitrides) of Nb, Cr, Ti, W or Si
574.2	Small	Cr metal or Cr_7C_3	574.2	Large	Cr metal or Cr_7C_3
576.5	Large	CrO_3	576.6	Trace	CrO_3
583.6	Small	Cr metal or Cr_7C_3	583.3	Medium	Cr metal or Cr_7C_3
586.2	Medium	CrO_2	–	–	–

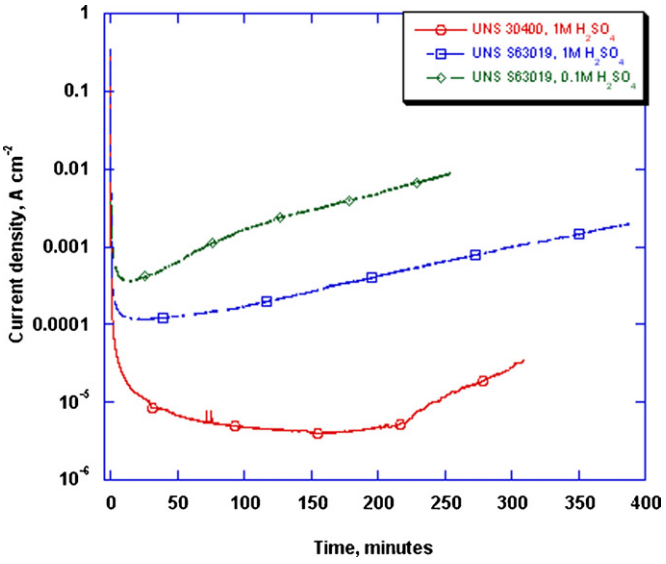

Fig. 9. Potentiostatic polarization of S30400 and S63019 in 1 M H_2SO_4 and S63019 in 0.1 M H_2SO_4 in an oxygen-saturated solution. The current density for S30400 is much lower than for S63019.

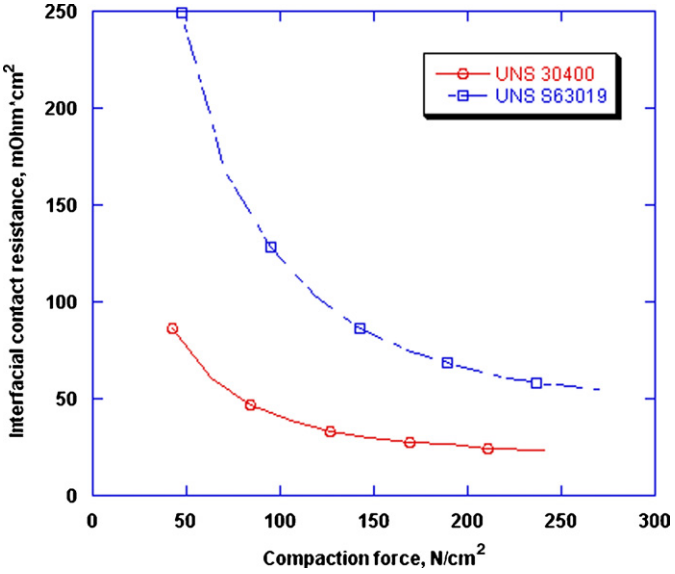

Fig. 11. Interfacial contact resistance measurements for S30400 and S63019. Electrical conductivity of the passive film on S30400 is significantly greater than that for S63019.

a passive chromium oxide surface layer. The fact that the polished surface of S63019 pitted when etched (Fig. 2) is further evidence of passive film inadequacy. Chromium carbides also tend to accumulate at grain boundaries and cause these locations to be susceptible to enhanced corrosion attack (Fig. 10). Reduced corrosion protection resulting from the extensive formation of chromium carbides,

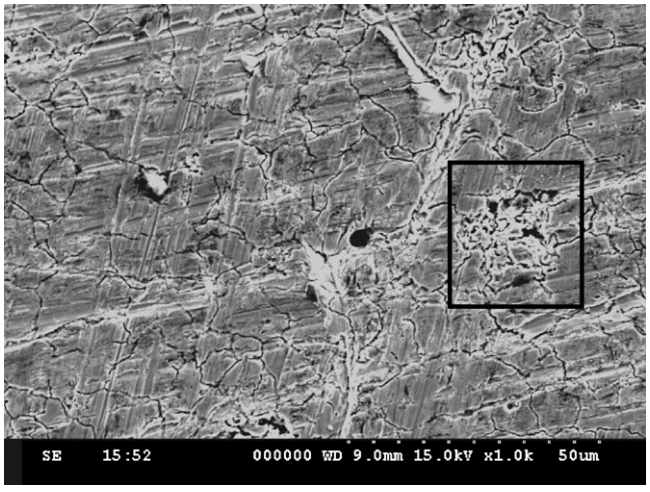

Fig. 10. S63019 after 5.6 h exposed to simulated cathodic PEMFC environment, 0.1 M H_2SO_4. Intergranular cracking is widespread along with corrosion at clusters of chromium carbides (box).

and possibly manganese carbides as well [15], overshadowed any beneficial impact that nitrogen may have had in enhancing corrosion resistance.

No significant difference in corrosion resistance was determined between the electrochemical testing performed in 1 M and 0.1 M H_2SO_4. This may suggest that the corrosion reaction is diffusion-controlled, with either sulfuric acid solution providing hydrogen ions for the cathodic reaction at an equally rapid rate in the turbulent solution.

The presence of niobium did not provide an enhanced electrically conductive pathway through the surface oxide on S63019. Much of the niobium was bound with carbon, which should have resulted in an electrically conductive NbC_x compound [4]. The relatively poor ICR performance of S63019 in comparison with S30400 was likely due to a combination of an increased presence of non-conductive iron oxides on the alloy surface (due to less available chromium oxide to form a passive film), and to an effective lack of conductivity of the NbC_x particles embedded in the alloy by the formation of relatively non-conductive NbO_x compounds on their surfaces.

4. Conclusions

S63019 did not perform well with regard to either surface oxide conductivity or corrosion resistance in the simulated PEMFC environment. The potential benefit of elevated nitrogen concentration was overshadowed by the lack of adequate free chromium in the alloy to produce a passive oxide and to protect grain boundaries

from corrosion. Segregated niobium particles present as NbC_x did not enhance electrical conductivity in the passive oxide film due to formation of an electrically insulating niobium oxide layer.

Acknowledgements

Valuable technical input was provided by David Olson and Timothy Ohno of the Colorado School of Mines.

References

[1] H. Tawfik, Y. Hung, D. Mahajan, J. Power Sources 163 (2007) 755.
[2] A. Hermann, T. Chaudhuri, P. Spagnol, Int. J. Hydrogen Energy 30 (2005) 1297–1302.
[3] W. Lai, W. Zhao, F. Wang, C. Qi, J. Zhang, Surf. Interface Anal. 41 (2009) 531.
[4] M. Kumagai, S.T. Myung, R. Asaishi, Y. Katada, H. Yashiro, J. Power Sources 185 (2008) 815.
[5] S.H. Lee, J.H. Kim, M.C. Kim, D.M. Wee, J. Power Sources 187 (2009) 312.
[6] R.J. Tian, J.C. Sun, L. Wang, J. Power Sources 163 (2007) 719.
[7] K.S. Weil, G. Xia, Z.G. Yang, J.Y. Kim, Int. J. Hydrogen Energy 32 (2007) 3724.
[8] M.P. Brady, H. Wang, B. Yang, J.A. Turner, M. Bordignon, R. Molins, M.A. Elhamid, L. Lipp, L.R. Walker, Int. J. Hydrogen Energy 32 (2007) 3778.
[9] B. Yang, M.P. Brady, H. Wang, J.A. Turner, K.L. More, D.J. Young, P.F. Tortorelli, E.A. Payzant, L.R. Walker, J. Power Sources 174 (2007) 228.
[10] S. Joseph, J.C. McClure, R. Chianelli, P. Pich, P.J. Sebastian, Int. J. Hydrogen Energy 30 (2005) 1339.
[11] H. Wang, G. Teeter, J.A. Turner, J. Fuel Cell Sci. Technol. 7 (2010) 021018–021021.
[12] M. Kumagai, S.T. Myung, S. Kuwata, R. Asaishi, Y. Katada, H. Yashiro, Electrochim. Acta 54 (2009) 1127.
[13] V.G. Gavriljuk, H. Berns (Eds.), High Nitrogen Steels: Structure, Properties, Manufacture, Applications, Springer-Verlag, Berlin, 1999.
[14] H. Wang, M.A. Sweikart, J.A. Turner, J. Power Sources 115 (2003) 243.
[15] V. Lazic, D. Milosavljevic, S. Aleksandrovic, P. Marinkovic, G. Bogdanovic, B. Nedeljkovic, Tribol. Rev. 32 (2010) 11.